

# The Role of Electron-electron Interactions in Graphene ARPES Spectra

Marco Polini,<sup>1,\*</sup> Reza Asgari,<sup>2</sup> Giovanni Borghi,<sup>1</sup> Yafis Barlas,<sup>3</sup> T. Pereg-Barnea,<sup>3</sup> and A.H. MacDonald<sup>3</sup>

<sup>1</sup>*NEST-CNR-INFM and Scuola Normale Superiore, I-56126 Pisa, Italy*

<sup>2</sup>*Institute for Studies in Theoretical Physics and Mathematics, Tehran 19395-5531, Iran*

<sup>3</sup>*Department of Physics, The University of Texas at Austin, Austin Texas 78712*

We report on a theoretical study of the influence of electron-electron interactions on ARPES spectra in graphene that is based on the random-phase-approximation and on graphene's massless Dirac equation continuum model. We find that level repulsion between quasiparticle and plasmaron resonances gives rise to a gap-like feature at small  $k$ . ARPES spectra are sensitive to the electron-electron interaction coupling strength  $\alpha_{\text{gr}}$  and might enable an experimental determination of this material parameter.

PACS numbers: 72.10.-d,73.21.-b,73.50.Fq

*Introduction*— In quasi two-dimensional (2D) crystals ARPES is a powerful probe of band structure and of Coulomb and phonon-mediated electron-electron interactions. A number of recent experiments [1] have reported ARPES spectra for single-layer and bilayer graphene systems grown epitaxially [2] on the surface of SiC. These recently isolated [3] 2D crystals have attracted considerable attention because of unusual properties [4, 5] that follow from chiral band states, notably unusual quantum Hall effects [6], and because of potential for applications. Experiment appears to establish [1] that both electron-phonon and electron-electron dressings have an influence on graphene's ARPES spectra. Recent theoretical studies [7, 8, 9] provide a solid basis for interpreting the electron-phonon contributions; in this Letter we report on a theoretical study of the influence of electron-electron interactions. Our analysis is based on the massless Dirac model which describes [10] the  $\pi$  electron states within  $\sim 2\text{eV}$  of the Fermi energy of a neutral graphene sheet and on the random phase approximation (RPA) for the self-energy.

The self-energy in a system of fermions is naturally separated into an exchange contribution due to interactions with occupied states in the static Fermi sea, and a correlation contribution due to quantum fluctuations of the Fermi sea [11]. Graphene differs [12] from the widely studied 2D systems in semiconductor quantum wells because its quasiparticles are chiral and because it is gapless and therefore has interband quantum fluctuations on the Fermi energy scale. In graphene band eigenstate chirality endows exchange interactions with a new source of momentum dependence which renormalizes the quasiparticle velocity and strongly influences the compressibility and the spin-susceptibility [13, 14, 15].

Our results [16] for the ARPES spectra of a n-doped graphene sheet with  $\alpha_{\text{gr}} = 2$  are summarized in Fig. 1. Here  $\alpha_{\text{gr}} = ge^2/\epsilon\hbar v$  is the interaction coupling strength,  $g = g_{\text{spin}}g_{\text{valley}} = 4$  is a band degeneracy factor,  $v$  is the Fermi velocity, and  $\epsilon$  depends on the dielectric environment of the graphene layer ( $\alpha_{\text{gr}} \sim 2$  is a typical value thought to apply to graphene sheets on the surface of a

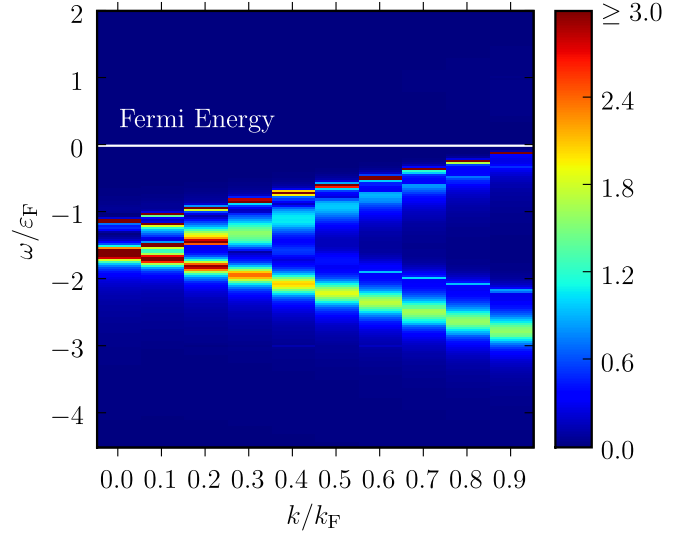


FIG. 1: (Color online) Spectral function  $\mathcal{A}(\mathbf{k}, \omega)$  of a n-doped graphene sheet for with wavevector  $k$  in units of Fermi wavevector  $k_F$  and energy  $\omega$  in units of and measured from the Fermi energy  $\hbar v k_F$ . The ARPES spectra for each  $k$  is the portion of the spectral function with  $\omega < 0$ . The  $k$ -dependence is represented in this figure by results for ten discrete  $k \in [0.0, 0.9]$  values separated by 0.1. It follows from particle-hole symmetry that the spectral function of a p-doped graphene sheet is specified by the  $\omega > 0$  spectral weight.

SiO<sub>2</sub> substrate). The most notable aspect of these results is the appearance near  $k = 0$  of strong plasmaron peaks in addition to quasiparticle peaks, which give rise to a gap-like structure in the overall spectrum. In the following paragraphs we explain the physics behind this figure.

*Doped Dirac Sea Charge Fluctuations*— The massless Dirac band Hamiltonian of graphene is [5]

$$\mathcal{H} = v\tau(\sigma_1 p_1 + \sigma_2 p_2), \quad (1)$$

where  $\tau = \pm 1$  for the inequivalent  $K$  and  $K'$  valleys at which  $\pi$  and  $\pi^*$  bands touch,  $p_i$  is an envelope function momentum operator, and  $\sigma_i$  is a Pauli matrix which

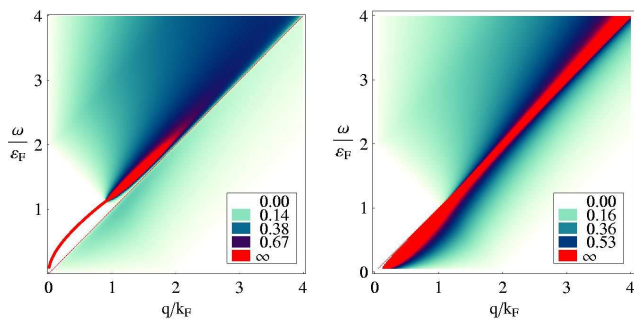


FIG. 2: (Color online) Left panel:  $-\Im m[\varepsilon^{-1}(\mathbf{q}, \omega)]$  as a function of  $q/k_F$  and  $\omega/\varepsilon_F$  for  $\alpha_{\text{gr}} = 2$ . The red solid line is the plasmon dispersion relation,  $\omega_{\text{pl}}(q \rightarrow 0) = \varepsilon_F \sqrt{\alpha_{\text{gr}} q / (2k_F)}$ . Right panel:  $-v_q \Im m[\chi^{(0)}(\mathbf{q}, \omega)]$  as a function of  $q/k_F$  and  $\omega/\varepsilon_F$ . The left and right panels become identical in the non-interacting  $\alpha_{\text{gr}} \rightarrow 0$  limit.

acts on the sublattice pseudospin degree-of-freedom. The low-energy valence band states have pseudospin aligned with momentum, while the high energy conduction band states, split by  $2v|\mathbf{p}|$ , are anti-aligned. In Fig. 2 we compare the particle-hole excitation [14, 17] spectra of non-interacting and interacting 2D doped Dirac systems. The non-interacting particle-hole continuum is represented here by the imaginary part of graphene's Lindhard function,  $\Im m[\chi^{(0)}(\mathbf{q}, \omega)]$ , which weighs transitions by the strength of the density fluctuation to which they give rise; transitions between states with opposite pseudospin orientation therefore have zero weight. More generally the band-chirality related density-fluctuation weighting factor (called the chirality factor below), which plays a key role in the physics of the ARPES spectra, is  $[1 \pm \cos(\theta_{\mathbf{k}, \mathbf{k}+\mathbf{q}})]/2$  with the plus sign applying for intraband transitions and the minus sign applying for inter-

band transitions, and  $\theta_{\mathbf{k}, \mathbf{k}+\mathbf{q}}$  equal to the angle between the initial state ( $\mathbf{k}$ ) and final state ( $\mathbf{k} + \mathbf{q}$ ) momenta. The weight is therefore high for intraband (interband) transitions when  $\mathbf{k}$  and  $\mathbf{k} + \mathbf{q}$  are in the same (opposite) direction. The main features in Fig. 2 that are important for ARPES spectra are the  $1/\sqrt{vq - \Omega}$  divergence which occurs near the upper limit of the  $q < k_F$  intraband particle-hole continuum and the relatively weak weight at the lower limit of the  $q < k_F$  inter-band particle-hole spectrum. The divergence at the intraband particle-hole spectrum contrasts with the singular but finite  $\sqrt{\Omega_{\text{max}} - \Omega}$  behavior at the upper end of the particle-hole continuum in an ordinary electron gas. The difference follows from the linear quasiparticle dispersion which places the maximum intraband particle-hole excitation energy at  $vq$  for all  $k$  in the Fermi sea.

In the RPA, quasiparticles interact with Coulomb-coupled particle-hole excitations. Because the bare particle-hole excitations are more sharply bunched in energy, Coulomb coupling leads to plasmon excitations that are sharply defined out to larger wavevectors than in the ordinary electron gas and steal more spectral weight from the particle-hole continuum. As seen in Fig. 2, the plasmon excitation of the Dirac sea remains remarkably well defined even when it enters the interband particle-hole continuum. The persistence occurs because transitions near the bottom of the interband particle-hole continuum have nearly parallel  $\mathbf{k}$  and  $\mathbf{k} + \mathbf{q}$  and therefore little charge-fluctuation weight. Interactions between quasiparticles and plasmons are stronger in the 2D massless Dirac system than in an ordinary non-relativistic 2D system.

*Dirac Quasiparticle Decay*— In Fig. 3 we plot our results for the imaginary part of the Dirac sea self-energy for a series of  $\mathbf{k}$  values (these results are for a n-doped  $\alpha_{\text{gr}} = 2$  system). In the RPA

$$\Im m[\Sigma_s(\mathbf{k}, \omega)] = \sum_{s'} \int \frac{d^2 \mathbf{q}}{(2\pi)^2} v_q \Im m[\varepsilon^{-1}(\mathbf{q}, \omega - \xi_{s'}(\mathbf{k} + \mathbf{q}))] \left[ \frac{1 + ss' \cos(\theta_{\mathbf{k}, \mathbf{k}+\mathbf{q}})}{2} \right] [\Theta(\omega - \xi_{s'}(\mathbf{k} + \mathbf{q})) - \Theta(-\xi_{s'}(\mathbf{k} + \mathbf{q}))] \quad (2)$$

where  $s, s' = \pm 1$  are band indices,  $v_q = 2\pi e^2 / (\epsilon q)$  is the 2D Coulomb interaction,  $\varepsilon(\mathbf{q}, \omega) = 1 - v_q \chi^{(0)}(\mathbf{q}, \omega)$  is the RPA dielectric function, and  $\Theta(x)$  is the Heaviside step function. The two factors in square brackets on the right-hand-side of Eq. (2) express respectively the influence of chirality and Fermi statistics on the decay process. Note that  $\Sigma_s$  depends on the band-index  $s$  only through the chirality factor. For  $\omega > 0$  and fixed  $\mathbf{q}$ , the RPA decay process represents scattering of an electron from momentum  $\mathbf{k}$  and energy  $\omega$  to  $\mathbf{k} + \mathbf{q}$  and  $\xi_{s'}(\mathbf{k} + \mathbf{q})$ , with all energies in Eq. (2) measured from the Fermi

energy. Since the Pauli exclusion principle requires that the final state is unoccupied, it must lie in the conduction band, *i.e.*  $s' = +1$ . Furthermore since the Fermi sea is initially in its ground state, the quasiparticle must lower its energy, *i.e.*  $\xi_{s'} < \omega$  – electrons decay by going down in energy. For  $\omega < 0$ , the self-energy expresses the decay of holes inside the Fermi sea, which scatter to a final state, by exciting the Fermi sea. In this case the final state must be occupied so both band indices are allowed for  $s'$ , and energy conservation requires that holes decay by moving up in energy. Since photoemission measures the

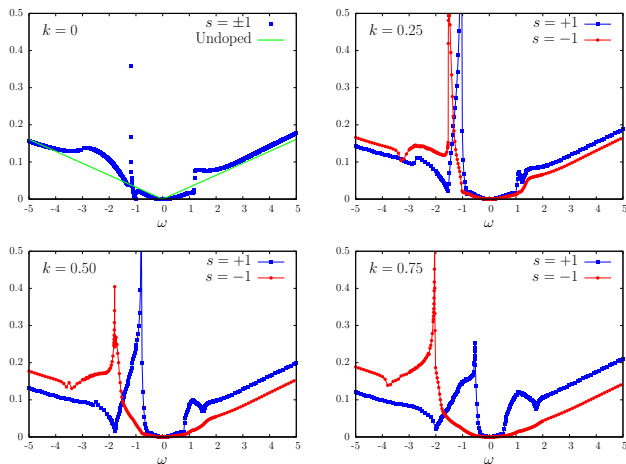


FIG. 3: (Color online) The absolute value  $|\Im m[\Sigma_s(\mathbf{k}, \omega)]|$  of the imaginary part of the RPA quasiparticle self-energy (in units of  $\varepsilon_F$ ) of an n-doped system as a function of energy  $\omega$  for  $k = 0, 0.25, 0.50$ , and  $0.75$  and for  $\alpha_{\text{gr}} = 2$ .

properties of holes produced in the Fermi sea by photo ejection, only  $\omega < 0$  is relevant for this experimental probe. Note however that because of the particle-hole symmetry properties of the Dirac model  $\Sigma_s(\mathbf{k}, \omega)$  in an n-doped system is identical to  $\Sigma_{-s}(\mathbf{k}, -\omega)$  in a system with the opposite doping. Our results for  $\Im m[\Sigma_s(\mathbf{k}, \omega)]$  for  $\omega > 0$ , therefore specify the ARPES spectra of p-doped graphene.

We remark that because interaction and band energies in graphene's Dirac model both scale inversely with length,  $\Im m[\Sigma_s(\mathbf{k}, \omega)] = vk_F F(\omega/vk_F, k/k_F)$ . For large  $|x|$ ,  $F(x, y) \rightarrow -\pi\alpha_{\text{gr}}^2 \ell(\alpha_{\text{gr}})|x|/(64g)$ , where

$$\ell(\alpha_{\text{gr}}) = \int_0^1 dx \frac{x\sqrt{1-x}}{1-x + \pi^2\alpha_{\text{gr}}^2 x^2/256} \quad (3)$$

$[\ell(0) = 4/3, \ell(2) \simeq 0.655124]$ . This implies that for  $|\omega| \gg vk_F$ , the decay rate in a doped system ( $\Im m[\Sigma_s(\mathbf{k}, \omega)]$ ) approaches that of an undoped system (the Fermi energy  $\varepsilon_F = vk_F$  is used as the energy unit and  $k_F$  as the unit of wavevector in all plots and in the remaining sections of this Letter). As we will see, however, the doped system properties are quite different from those of an undoped system up to energy scales several times larger than the Fermi energy, particularly so near the Dirac ( $k = 0$ ) point.

In explaining the spectra plotted in Fig. 3 we start with the  $k = 0$  case ( $\Im m[\Sigma_+(0, \omega)] = \Im m[\Sigma_-(0, \omega)]$ ) for which the final state energy is  $\xi_{s'}(\mathbf{q}) = s'q - 1$ . For  $\omega > 0$  the final state must be unoccupied so that  $s' = +1$ ;  $q$  is restricted to those values larger than 1 for which the Dirac sea excitation energy  $\Omega(q) = \omega + 1 - q$  is positive. Comparing with Fig. 2 we see that  $\Im m[\Sigma_+(0, \omega)]$  vanishes like  $\omega^2$  for  $\omega \rightarrow 0$ , a universal property of normal Fermi

liquids. In the RPA

$$\Im m[\Sigma_+(0, \omega \rightarrow 0)] = -\frac{\sqrt{3}}{8g} \frac{\alpha_{\text{gr}}^2}{(1 + \alpha_{\text{gr}})^2} \omega^2. \quad (4)$$

The sharp increase in  $\Im m[\Sigma_+(0, \omega)]$  which occurs at  $\omega \sim 1.2$  reflects the onset of plasmon emission. Note that these plasmons at  $q > 1$  remain well defined excitations well into the interband particle-hole continuum. For  $\omega < 0$ , relevant to ARPES in n-doped graphene, both conduction and valence band final states occur and transitions are allowed if the transition energy  $\Omega(q) = |\omega| - 1 + s'q$  is positive and the final hole state is occupied, *i.e.*  $q < 1$  for  $s' = +$ . Note that for final states in the conduction band, the transition energy is close to the plasmon excitation energy over a wide range of  $q$  values. This property leads to much stronger plasmon features for  $\omega < 0$  than for  $\omega > 0$ .  $\Im m[\Sigma_+(0, \omega)]$  diverges for  $\omega \sim -1.3$ , the value at which  $\Omega(q)$  for  $s' = +1$  is tangent to the plasmon dispersion line illustrated in Fig. 2. In this case, the hole scatters into a resonance consisting of a quasiparticle strongly coupled to plasmon excitations, a plasmaron [18, 19]. At finite  $k$ , the conduction and valence band  $\Im m[\Sigma_s(\mathbf{k}, \omega)]$  plasmaron peaks broaden and separate, because of the dependence on scattering angle of  $\xi_{s'}(\mathbf{k} + \mathbf{q})$  and because of chirality factors which emphasize  $\mathbf{k}$  and  $\mathbf{q}$  in nearly parallel directions for conduction band states and  $\mathbf{k}$  and  $\mathbf{q}$  in nearly opposite directions for valence band states. Because of the chirality factor the conduction band plasmaron moves up in energy approximately as  $vk$  while the valence band plasmaron moves down.

*ARPES Spectra*—We are now prepared to discuss the ARPES spectra in Fig. 1. ARPES measures the wavevector dependent electron spectral function

$$\mathcal{A}_s(\mathbf{k}, \omega) = \frac{1}{\pi} \frac{|\Im m \Sigma_s(\mathbf{k}, \omega)|}{[\omega - \xi_s(\mathbf{k}) - \Re e \Sigma_s(\mathbf{k}, \omega)]^2 + [\Im m \Sigma_s(\mathbf{k}, \omega)]^2}. \quad (5)$$

Near the Fermi energy the spectral function consists of a narrow Lorentzian centered at the energy  $E$  which solves the Dyson equation for the quasiparticle energy:

$$E = \xi_s(\mathbf{k}) + \Re e \Sigma_s(\mathbf{k}, E). \quad (6)$$

For small  $k$  we see in Fig. 4 that there are two solutions to this equation, which are shifted from the bare quasiparticle energy and the plasmaron energy because of the strong energy-dependence of  $\Re e \Sigma_s$  near the  $\Im m \Sigma_s$ 's plasmaron peak. These shifts can be understood as following from level repulsion between a bare particle resonance and a plasmaron resonance. We also note in Fig. 4 that  $\Re e \Sigma_s$  has a negative contribution which is present at the Fermi energy and persists over a wide regime of energy. This contribution is due to exchange and correlation interactions of quasiparticles near the Fermi energy with the negative energy sea. As explained [12, 14, 20] previously, this effect produces a nearly rigid shift in the

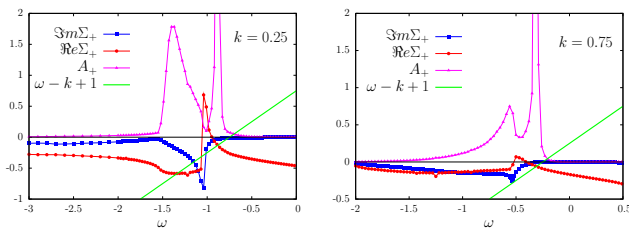


FIG. 4: (Color online)  $\Re[\Sigma_+(\mathbf{k}, \omega)]$ ,  $\Im[\Sigma_+(\mathbf{k}, \omega)]$ , and spectral function  $\mathcal{A}_+(\mathbf{k}, \omega)$  for  $k = 0.25$  and  $k = 0.75$ . The band energy and  $\Re\Sigma_+$  are measured from the band  $\varepsilon_F$  and interaction  $[\Sigma_+(k_F, \omega = 0)]$  contributions to the chemical potential.

band energies which is increasingly negative further below the Fermi energy, increasing the band dispersion and the quasiparticle velocity. In Fig. 4 we show that for larger  $k$ , the plasmaron feature in  $\Im\Sigma_s$  is broadened sufficiently to remove the plasmaron solution of the quasiparticle Dyson equation. In this limit, the spectral function has only a weak plasmon satellite on top of the main quasiparticle peak.

The full ARPES spectral in Fig. 1 can be understood by applying considerations like those explained above to both bands and over the full range of  $k$ . Because the negative exchange-correlation shift in the quasiparticle energy gets larger as  $k \rightarrow 0$  in the conduction band, the energy splitting between the sharpening plasmaron resonance and the band-like quasiparticle decreases and their coupling increases. In addition, because the slope difference between  $E - \xi_s(\mathbf{k})$  and  $\Re\Sigma_s(\mathbf{k}, E)$  is smaller at the plasmaron Dyson equation solution than at the quasiparticle Dyson equation solution, the plasmaron assumes the larger fraction of the spectral weight. The detailed behavior near  $k = 0$  is sensitive to the value of  $\alpha_{gr}$ . For  $\alpha_{gr} = 2$ , the avoided crossing between quasiparticle and plasmaron solutions occurs near  $k = 0$ . Because the higher energy valence band peak has little spectral weight when it crosses the Fermi energy, the overall spectrum can appear to have an energy gap.

Because electron-electron interaction effects occur on the  $vk_F$  energy scale they can be separated from electron-phonon interaction effects experimentally by varying carrier density. Although the RPA is not exact, it provides a good starting point for interpreting the influence of electron-electron interactions on the ARPES spectra of graphene sheets. As we have shown, the downward shift of valence band states compared to conduction band states and plasmaron-quasiparticle level repulsion and weight transfer effects must be accounted for to interpret ARPES data. Features in the data which might otherwise be interpreted as extrinsic effects related to disorder or interactions with substrates can have interesting and subtle intrinsic origins. Close comparison between theory and experiment and further materials progress will

augment the power of ARPES experiments.

*Acknowledgment* — This work has been supported by the Welch Foundation, by the Natural Sciences and Engineering Research Council of Canada, by the Department of Energy under grant DE-FG03-02ER45958, and by the National Science Foundation under grant DMR-0606489. We thank Alessandra Lanzara, Steve Louie, and Andrea Tomadin for helpful discussions.

\* Electronic address: m.polini@sns.it

- [1] E. Rollings *et al.*, J. Phys. Chem. Solids **67**, 2172 (2006); A. Bostwick *et al.*, Nat. Phys. **3**, 36 (2007).
- [2] For a review on the properties of epitaxial graphene see W.A. de Heer *et al.*, Solid State Commun. **143**, 92 (2007).
- [3] K.S. Novoselov *et al.*, Science **306**, 666 (2004).
- [4] A.K. Geim and K.S. Novoselov, Nat. Mat. **6**, 183 (2007); M.I. Katnelson and K.S. Novoselov, Solid State Commun. **143**, 3 (2007).
- [5] For a recent popular review see A.K. Geim and A.H. MacDonald, Physics Today, vol. page (2007).
- [6] K.S. Novoselov *et al.*, Nature **438**, 197 (2005); Y.B. Zhang *et al.*, Nature **438**, 201 (2005).
- [7] M. Calandra and F. Mauri, arXiv:0707.1467v1.
- [8] C.-H. Park, F. Giustino, M.L. Cohen, and S.G. Louie, arXiv:0707.1666v1.
- [9] W.-K. Tse and S. Das Sarma, arXiv:0707.3651v1.
- [10] T. Ando, T. Nakanishi, and R. Saito, J. Phys. Soc. Japan **67**, 2857 (1998).
- [11] G.F. Giuliani and G. Vignale, *Quantum Theory of the Electron Liquid* (Cambridge University Press, Cambridge, 2005).
- [12] M. Polini *et al.*, Solid State Commun. **143**, 58 (2007).
- [13] J. Gonzales, F. Guinea, and M.A.H. Vozmediano, Phys. Rev. B **59**, 2474 (1999); M.I. Katsnelson, Eur. Phys. J. B **52**, 151 (2006); E.G. Mishchenko, Phys. Rev. Lett. **98**, 216801 (2007); O. Vafek, *ibid.* **98**, 216401 (2007); S. Das Sarma, E.H. Hwang, and W.-K. Tse, Phys. Rev. B **75**, 121406(R) (2007); X.-Z. Yan and C.S. Ting, arXiv:0705.2752v1; D.E. Sheehy and J. Schmalian, arXiv:0707.2945v1.
- [14] Y. Barlas *et al.*, Phys. Rev. Lett. **98**, 236601 (2007).
- [15] E.H. Hwang, B.Y.-K. Hu, and S. Das Sarma, cond-mat/0612345.
- [16] This information is available in numerical form upon request to the authors.
- [17] K.W.-K. Shung, Phys. Rev. B **34**, 979 (1986); B. Wunsch, T. Stauber, F. Sols, and F. Guinea, New J. Phys. **8**, 318 (2006); X.-F. Wang and T. Chakraborty, Phys. Rev. B **75**, 033408 (2007); E.H. Hwang and S. Das Sarma, *ibid.* **75**, 205418 (2007).
- [18] L. Hedin, Phys. Rev. **139**, A796 (1965).
- [19] R. Jalabert and S. Das Sarma, Phys. Rev. B **40**, 9723 (1989).
- [20]  $\Re\Sigma_s$  is weakly dependent on the massless Dirac model's ultraviolet cutoff  $\Lambda$  [12, 14]. For this reason the spectral function  $\mathcal{A}_s(\mathbf{k}, \omega)$  is not exactly a function of only  $k/k_F$  and  $\omega/\varepsilon_F$ . This caveat is of little practical significance however since deviations are very small over the two to three orders of magnitude of graphene sheet charge

density which lies the window between the low density cutoff  $\sim 10^{11}\text{cm}^{-2}$  below which disorder plays a strong role and the high density cutoff  $\sim 10^{14}\text{cm}^{-2}$  imposed by

fundamental gating and doping limitations. The numerical results shown in this work have been calculated with  $\Lambda = 10^2$ .